# Chapter 5

# Ru(III) Pyrimidine Schiff base complexes

## 5.1. Introduction

Ru complexes were first tested successfully for anti-cancer activity by Dwyer and coworkers in the 1950s[1]. In 1976, chloro-ammine Ru(III) complexes; *e.g.*, *fac*-$[Ru(NH_3)_3Cl_3]$ were found to induce filamentous growth of *Escherichia coli* cells, with comparable activity to cisplatin. Subsequently, *cis*-$[Ru(NH_3)_4Cl_2]$ was observed by Clarke in 1980 to show anticancer properties. Unfortunately, these complexes turned out to be too insoluble for pharmaceutical use[2-4]. Later on, the Keppler group introduced Ru(III) complexes that displayed activity against several screening tumor lines, especially significant results against Pt-resistant colorectal tumors in mice. Sava focused on complexes bearing the DMSO-ligand, which were effective against solid metastasizing tumors in mice. After much extensive research, two ruthenium complexes, imidazolium *trans*tetrachlorido(dimethylsulfoxide) imidazoleruthenate (III) (NAMI-A) (developed by Sava *et al.*) and indazolium (*trans*-tetrachloridoruthenate(III)) (KP1019) (developed by Keppler *et al.*) were found to display the highest potential as anti-cancer agents[5-8]. Although they look similar, the properties displayed were found to be very different. Both of these compounds have successfully completed Phase I clinical trials. However, further progress with KP1019 was hindered due to its poor aqueous solubility and the fact that the maximum tolerated dose and optimal dose could not be determined. This issue was solved by replacing the indazolium counter ion with sodium, and the new complex (called KP1339) is still undergoing clinical trials. The discovery of NAMI-A has been one of the most promising developments in metal-based anti-cancer drugs since cisplatin due to its strong anti-cancer properties and low toxicity. In continuation with the efforts of many researchers working in Ru(III) complexes as anticancer agents, we tend to synthesize pyrimidine Schiff base complexes and study their pharmacological activity.

## 5.2. Synthesis of Schiff base ligand

A mixture of 5,6-diamino-2-mercapto-*1H*-pyrimidin-4-one (0.15 g, 1 mmol), substituted aldehydes (1mmol) in 95% ethanol/DMF was refluxed for 2 h (Scheme 1). The reaction mixture was cooled to room temperature and the precipitate formed was filtered, washed with ethanol and recrystallised from DMF/ethanol mixture.

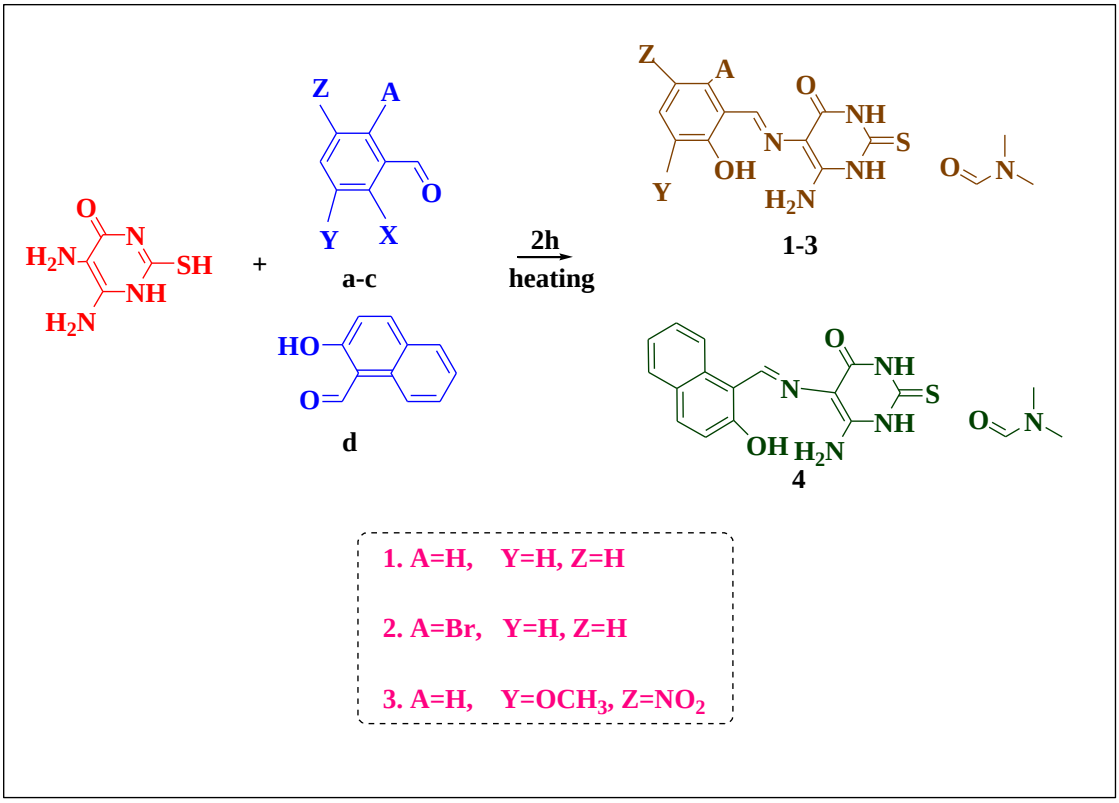


**Scheme 1: Synthesis of Schiff base ligands**

**5.2.1.*6-amino-5-[2-hydroxy-benzylidene)-amino]-2-thioxo-dihydro-pyrimidin-4-one(1) $L_1$:*** Crystallized from DMF/Ethanol; yield 78%; m.pt: 237-240 °C. Anal. calcd (%) for $C_{14}H_{16}N_5O_3S$ (334.38) : C, 49.84; H, 5.68; N, 20.76; found (%), C, 49.79; H, 5.63; N, 20.70, IR($cm^{-1}$): 1554(C=N); 1354(C=S), UV-vis(nm): 310, 415.$^1$H-NMR(ppm): δ6.76-8.15(m, 4H, aromatic); δ8.11(s, 1H, -CH=N pyrimidine ring), δ 4.54(s, 1H,-OH), δ7.86(s, 1H, >CH=N), δ11.57(s, 2H, -$NH_2$), δ13.17(s, 1H, H-C=O), δ2.90(s, 6H, 2$CH_3$). $^{13}$C-NMR (ppm): δ 115.8-157.8(aromatic), δ163.7 (-CH=N), δ168.3 (-C=O), δ89.5 (N-C=), δ161.8(C-$NH_2$), δ178.2(C=S), δ33.7 ($CH_3$), δ162 (H-C=O).

**5.2.2.*6-amino-5-[2-bromo-6-hydroxy-benzylidene)-amino]-2-thioxo-dihydro-pyrimidin-4-one (2) $L^2$:*** Crystallized from DMF/Ethanol; yield 75%; mp: 254-256 °C. Anal. calcd. (%) for $C_{14}H_{15}BrN_5O_3S$ (415.03): C, 40.39; H, 4.36; N: 16.82; found (%) : C, 40.31; H, 4.29; N: 16.76. IR ($cm^{-1}$): 1560(C=N); 1357 (C=S), UV-vis (nm): 325, 420. $^1$H-NMR(ppm): δ6.85-8.45(m, 3H, aromatic); δ8.52(s, 1H, -CH=N pyrimidine ring), δ 5.01(s, 1H,-OH), δ7.93(s, 1H, >CH=N), δ 11.67(s, 1H, amine –NH), δ4.57(s, 1H, -OH), δ13.97(s, 1H, H-C=O), δ2.90(s, 6H, 2$CH_3$). $^{13}$C-NMR (ppm): δ 114.8-

160.0(aromatic), δ163.7 (-CH=N), δ168.3 (-C=O), δ89.5 (N-C=), δ161.8(C-$NH_2$), δ178.2(C=S), δ33.7 ($CH_3$), δ162.0 (H-C=O).

**5.2.3.*6-amino-5-[(2-hydroxy-6-methoxy-4-nitro-benzylidene)amino]-2-thioxo-2,3-dihydro-1H-pyrimidin-4-one(3) $L^3$*:**

Crystallized from DMF/Ethanol; yield 65%; mp: 251°C. Anal. calcd. (%) for $C_{15}H_{17}N_6O_6S$ (409.13): C, 43.90; H, 4.42; N, 20.48, S, 7.81; found (%) : C, 43.85; H, 4.38; N, 20.49, S, 7.75. IR ($cm^{-1}$): 1564(C=N); 1345(C=S), UV-vis (nm): 225, 340, 410. $^1$H-NMR (ppm ): δ7.3-7.5(m, 2H, aromatic); δ8.56(s, 1H, -CH=N pyrimidine ring), δ 5.03(s, 1H,-OH), δ7.95 (s, 1H, >CH=N), δ 11.71(s, 1H, amine –$NH_2$), δ5.07(s, 1H, -OH), δ13.97(s, 1H, H-C=O), 3.73(s, 3H, -$OCH_3$), δ8.02(s, 1H, H-C=O), δ2.90(s, 6H, 2$CH_3$). $^{13}$C-NMR (ppm): δ 103.2-164.8 (aromatic), δ163.7 (-CH=N), δ168.3 (-C=O), δ89.5 (N-C=), δ161.8 (C-$NH_2$), δ178.2(C=S), δ 56.0 ($OCH_3$), δ33.7 ($CH_3$), δ162 (H-C=O).

**5.2.4.*6-amino-5-[(2-hydroxy-naphthalen-1-ylmethylene)-amino]-2-thioxo-dihydro-pyrimidin -4-one (4) $L^4$:***

Crystallized from DMF/Ethanol; yield 56%; mp: 265°C. Anal. calcd. (%) for $C_{18}H_{19}N_5O_3S$ (385.12) : C, 56.09; H, 4.97; N, 18.17, S, 8.32; found (%) : C, 56.17; H, 4.90; N, 18.13, S, 8.35. IR ($cm^{-1}$): 1578(C=N); 1347(C=S), UV-vis (nm): 225,350, 450. $^1$H-NMR (ppm): δ7.21-7.86(m, 5H, aromatic); δ8.54(s, 1H, -CH=N pyrimidine ring), δ 5.04(s, 1H,-OH), δ8.01(s, 1H, >CH=N), δ 11.74(s, 1H, amine –$NH_2$), δ8.02(s, 1H, H-C=O), δ2.90(s, 6H, 2$CH_3$). $^{13}$C-NMR (ppm): δ 117.7-153.7(aromatic), δ163.7 (-CH=N), δ168.3 (-C=O), δ89.5 (N-C=), δ161.8(C-$NH_2$), δ178.2(C=S), δ33.7 ($CH_3$), δ162.0 (H-C=O).

**5.3. Preparation of the complexes**

**5.3.1. Synthesis of [$RuCl_3(PPh_3)_3$]**

Ruthenium trichloridetrihydrate (0.2g) was taken in ethanol (20 ml) and concentrated HCl (2 ml) was added to it. To the above solution triphenylphosphine (0.8 g) was added. The solution was heated under reflux for about 5 minutes and then cooled. The resulting reddish brown crystals were separated, washed with ether and dried. m.pt: 158°C.

**5.3.2. *Synthesis of [$Ru(Cl)_2(PPh_3)(L^1)$](5)***

A methanolic solution (20 mL) containing $L^1$ **(1) (**1mmol) and [$RuCl_3(PPh_3)_3$] (1mmol) in benzene (20mL) were mixed and the resulting brown solution was refluxed for 8h (Scheme 2). The reaction mixture was then cooled to room

temperature, which resulted in the formation of brown colored crystalline precipitate which was filtered off and the purity was checked by TLC. This solid was crystallized from $CH_2Cl_2$/hexane mixture. Yield: 59%, mp: 276-278°C. Anal. calcd. (%) for $C_{32}H_{32}Cl_2N_5O_3PRuS$: C, 49.94; H, 4.19; N, 9.10; S, 4.17. found (%): C, 49.87; H, 4.15; N, 9.13; S, 4.12. EI-MS: found m/z= 769.64($M^+$); calcd m/z=769.05($M^+$). IR(KBr, $cm^{-1}$): 1522(C=N), 746 (C-S). UV-vis(DMSO) λmax, nm: 273, 360, 417, 628. EPR(300 K, g value): 2.30.

**5.3.3.** ***Synthesis of [Ru(Cl)$_2$(PPh$_3$)(L$^2$)](6)***

It was prepared using the same procedure as described for **5** replacing **1** by **2**. Brown colored crystalline powder was obtained. Yield: 64%. m.pt: 254-256°C. Anal. calcd. (%) for $C_{32}H_{31}BrCl_2N_5O_3PRuS$: C, 45.29; H, 3.68; N, 8.25; S, 3.78. found(%): C, 45.37; H, 3.65; N, 8.13; S, 3.62. EI-MS: found m/z= 775.52.($M^+$); calcd m/z=776.12($M^+$). IR(KBr, $cm^{-1}$): 1513(C=N), 733(C-S). UV-vis(DMSO)λmax, nm: 267, 356, 514. EPR(300 K, g value): 1.98.

**5.3.4.** ***Synthesis of [Ru(Cl)$_2$(PPh$_3$)(L$^3$)](7)***

It was prepared using the same procedure as described for **5** by using **3** instead of **1**. Brown colored crystalline powder was obtained. Yield: 67%. mp: 265-267°C. Anal. calcd. (%) for $C_{30}H_{27}Cl_2N_5O_5PRuS$: C, 46.64; H, 3.52; N, 9.06; S, 4.15. found(%): C, 46.37; H, 3.65; N, 8.13; S, 4.62. EI-MS: found m/z= 770.54($M^+$); calcd m/z=772.60($M^+$). IR (KBr, $cm^{-1}$): 1520(C=N), 733(C-S). UV-vis(DMSO)λmax, nm: 267, 356, 561. EPR(300 K, g value): 2.05.

**5.3.5.** ***Synthesis of [Ru(Cl)$_2$(PPh$_3$)(L$^4$)](8)***

It was prepared using the same procedure as described for **5** by replacing **1** by **4**. Brown coloured crystalline powder was obtained. Yield: 68%. mp: 263-265°C. Anal. calcd. (%) for $C_{32}H_{31}BrCl_2N_5O_3PRuS$: C, 45.29; H, 3.68; N, 8.25; S, 3.78. found(%): C, 45.37; H, 3.65; N, 8.13; S, 3.62. EI-MS: found m/z= 848.54 ($M^+$); calcd m/z=848.12($M^+$). IR(KBr, $cm^{-1}$): 1513(C=N), 733(C-S). UV-vis(DMSO)λmax, nm: 267, 356, 544. EPR(300 K, g value): 2.13.

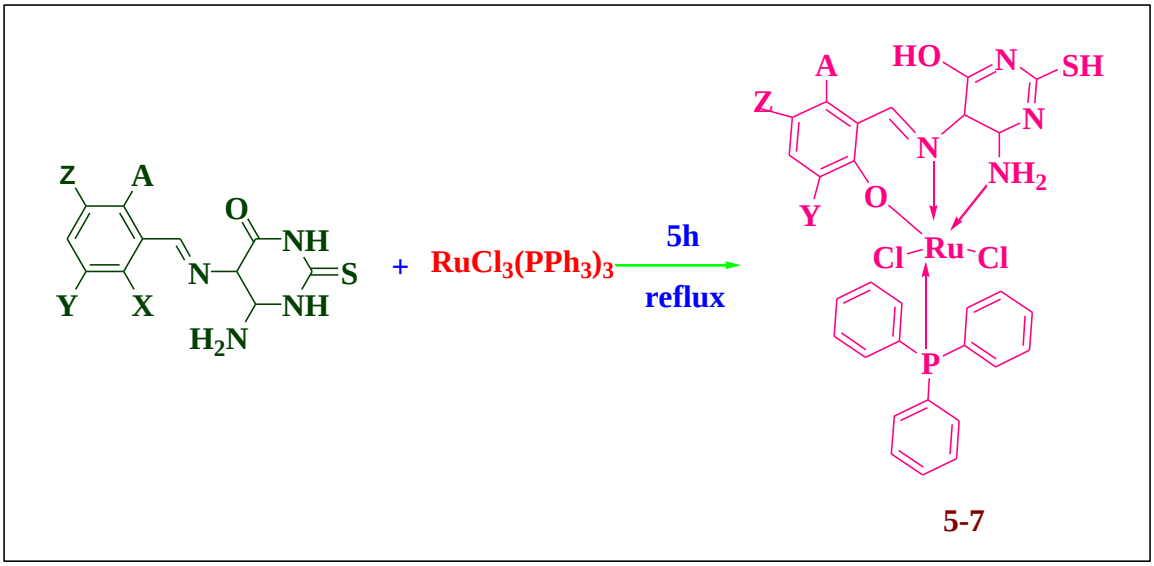


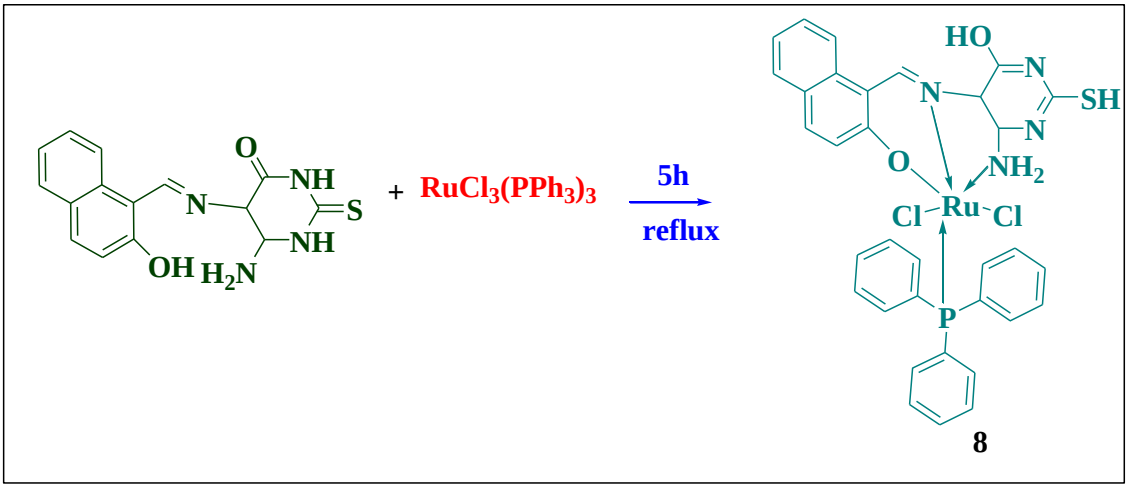


**Scheme 2: Synthesis of complexes**

The synthesized ruthenium complexes were characterized by spectral techniques and evaluated for their antimicrobial, anticancer antioxidant, DNA binding and catalytic activities.

### 5.4. Catalytic oxidation of alcohols

#### 5.4.1. $H_2O_2$ as oxidant

To a solution of alcohol (0.07-0.13 mL, 1 mmol) and dichloromethane (20 mL), $H_2O_2$ (0.09 ml, 3mmol) and the ruthenium complex (0.007g, 0.01 mmol) were added and the solution was heated under reflux for 3h. The mixture was then filtered and the filtrate was dried over anhydrous $Na_2SO_4$. It was then evaporated to dryness and extracted with diethyl ether. The diethyl ether extract was filtered and evaporated

to yield the corresponding carbonyl compound which was then quantified as its 2, 4-dinitrophenylhydrazone[9].

### 5.5. Results and Discussion

The reactions of various Schiff bases with $[RuCl_3(PPh_3)_3]$ yielded complexes of the general formula $[RuL^x(Cl)_2PPh_3]$. The complexes are non-hygroscopic and are soluble in common organic solvents such as $CH_2Cl_2$, $CHCl_3$, DMSO and DMF. In all the reactions, it was found that Schiff bases behave as a tridentate ligand replacing triphenylphosphine and $Cl^-$ ligands from the starting ruthenium precursors. The analytical data obtained for the new ruthenium(III) Schiff base complexes are given in experimental section and they agree very well with the proposed molecular formulae.

#### 5.5.1. FT-IR Spectra

The IR spectra of the free ligands were compared with those of the metal complexes in order to study the binding modes of the Schiff base ligands to metal (Table 5.1). A medium sharp band at 1546 to 1578 $cm^{-1}$ due to the azomethine C=N stretching frequency of the free ligands **1-4** respectively was shifted to lower frequency in the spectra of the complexes ranging between 15 to 35 $cm^{-1}$ proving that the azomethine nitrogen of the ligands is involved in co-ordination. A band appeared from 858 to 887 $cm^{-1}$ for the ligands due to the vibration of the C=S double bond which disappeared in the spectra of the complexes and a new band, C-S appeared at 733 to 748 $cm^{-1}$ indicating that the C=S has been enolised as thiolate sulphur[10]. In the ligands **1** to **4**, a band was observed around 3200 to 3500 $cm^{-1}$ for $\gamma(NH_2)$ asymmetric-symmetric bands, but in the complexes **5-8** these amine bands are not clear as the $–NH_2$ and –OH bands overlap in that region. The band ranging between 1729 and 1666 $cm^{-1}$ for **1-4** which are responsible for the carbonyl group in the pyrimidine ring vanished in the IR spectrum of the complexes showing that the group has been enolised and that is proved from the broad band in the region 3057 to 3189$cm^{-1}$. The C-O stretching frequency of the ligands range between 1100 and 1107$cm^{-1}$ which is shifted to higher wavelengths in the complexes 1156 to 1166$cm^{-1}$ showing that the phenolic –OH is involved in co-ordination. An additional C=N band appeared in the complexes around the region 1426 to 1435$cm^{-1}$ which is due to the C=N bond in the pyrimidine ring after the formation of S-H[11]. The ruthenium (III) Schiff base complexes show strong vibrations in the range 655-698, 1084-1107 and 1440-1458$cm^{-1}$ which are attributed to the triphenyl phosphine fragments[12]. The FT-IR spectra of the ligands and the complexes are given in Figs. 5.1a-h respectively.

**Table 5.1: FT-IR stretching frequencies of ligands and the complexes in $cm^{-1}$**

| Compounds | FT-IR stretching frequencies($cm^{-1}$) | | | | | | |
|---|---|---|---|---|---|---|---|
| | **$-NH_2$ / -OH** | **C=O** | **C=N** | **C-O** | **C=N (ring)** | **C=S** | **C-S** |
| **$L^1$** | 3201<br>3363 | 1729 | 1556 | 1104 | - | 1354 | - |
| **$L^2$** | 3223<br>3369 | 1657 | 1546 | 1100 | - | 1357 | - |
| **$L^3$** | 3221<br>3378 | 1713 | 1564 | 1103 | - | 1345 | - |
| **$L^4$** | 3220<br>3380 | 1710 | 1578 | 1107 | - | 1347 | - |
| **$[Ru(Cl)_2(PPh_3)(L^1)]$** | - | - | 1522 | 1156 | 1428 | - | 746 |
| **$[Ru(Cl)_2(PPh_3)(L^2)]$** | - | - | 1513 | 1166 | 1432 | - | 733 |
| **$[Ru(Cl)_2(PPh_3)(L^3)]$** | - | - | 1520 | 1158 | 1429 | - | 748 |
| **$[Ru(Cl)_2(PPh_3)(L^4)]$** | - | - | 1531 | 1159 | 1426 | - | 739 |

### 5.5.2. Electronic spectra

The electronic spectra of the ligands and the complexes were recorded in DMSO. The spectra of the free ligands show two types of transitions , the first at range 225 to 350nm assigned to $\pi \rightarrow \pi^*$ transitions due to molecular orbitals located on the phenolic chromophore. These peaks shift in the spectra of the complexes, due to donation of a lone pair of electrons from phenoxy oxygen to ruthenium. This reveals that one coordination site is phenolic oxygen. The second type of transition appeared at 410 to 420nm assigned to $n \rightarrow \pi^*$ transition due to the azomethine groups[13].

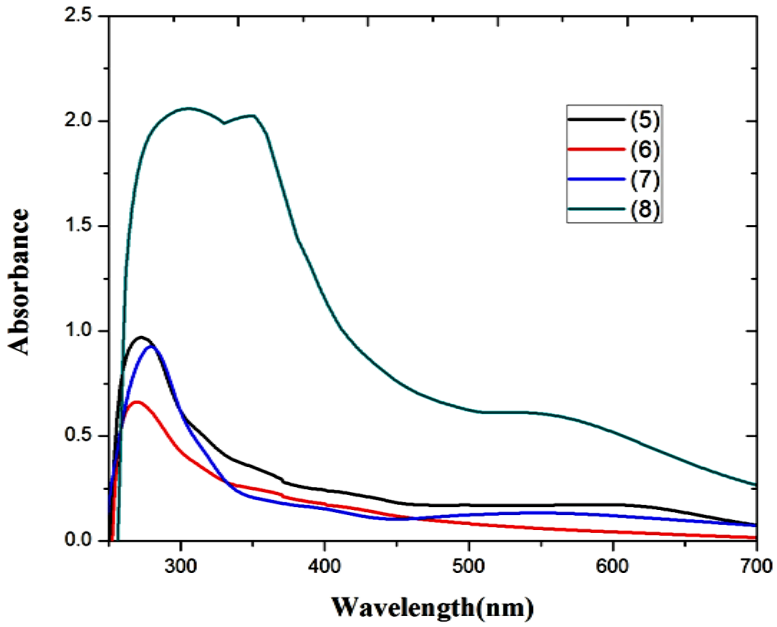


**Fig. 5. 2. Electronic spectra of Ru(III) complexes**

**Table 5. 2. Electronic spectra of the ligand and the complexes in nm**

| **Compound** | **UV spectral bands (nm)** | **Band Assignments** | **Geometry** |
|---|---|---|---|
| **$L^1$** | 225, 355, 415 | n-π*, π-π* | - |
| **$L^2$** | 225,345, 420 | n-π*, π-π* | - |
| **$L^3$** | 225, 340,410 | n-π*, π-π* | - |
| **$L^4$** | 225,350,450 | n-π*, π-π* | - |
| **$[Ru(Cl)_2(PPh_3)(L^1)]$** | 273,360<br>417,628 | Charge transfer<br>$^2T_{2g}\rightarrow{}^4T_{2g}$, $^2T_{2g}\rightarrow{}^2A_{1g}$ | **Octahedral** |
| **$[Ru(Cl)_2(PPh_3)(L^2)]$** | 267,356<br>514 | Charge transfer<br>$^2T_{2g}\rightarrow{}^2A_{1g}$ | **Octahedral** |
| **$[Ru(Cl)_2(PPh_3)(L^3)]$** | 286,376,<br>561 | Charge transfer<br>$^2T_{2g}\rightarrow{}^2A_{1g}$ | **Octahedral** |
| **$[Ru(Cl)_2(PPh_3)(L^4)]$** | 294,353<br>544 | Charge transfer<br>$^2T_{2g}\rightarrow{}^2A_{1g}$ | **Octahedral** |

These bands also shift in the spectra of the new complexes, indicating the involvement of imine nitrogen in co-ordination with ruthenium. The spectra of all the complexes showed transitions, different from that of the free ligands around 350 to 650nm. In most ruthenium(III) complexes, the electronic spectra shows apart from

intra-ligand transitions, three sets of bands present with wavelength ranging from 500-600nm corresponding to $^2T_{2g} \rightarrow {}^4T_{1g}$ transitions of the metal 'd' orbitals. Similarly, bands in the wavelength range 400-500 nm and 380-400 nm were assigned to $^2T_{2g} \rightarrow {}^4T_{2g}$ and $^2T_{2g} \rightarrow {}^2A_{1g}$, transitions of the metal d orbitals respectively[14]. The electronic spectra of the complexes are shown in Fig. 5.2 and the transitions are given in Table 5. 2.

### 5.5.3. Magnetic moment and EPR spectra

The room temperature magnetic susceptibility measurement of the ruthenium (III) complexes shows that they are paramagnetic. The magnetic moment value $\mu_B$ = 1.64-2.30 corresponds to single unpaired electron in a low spin $4d^5$ configuration and confirms that ruthenium is in +3 oxidation state in all the complexes.

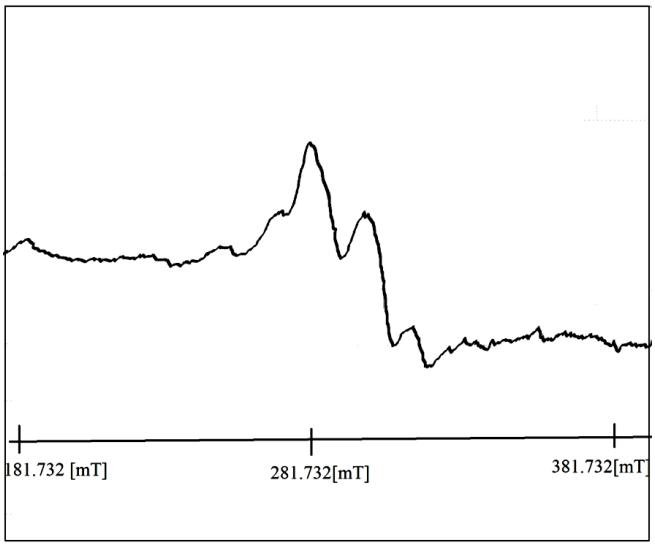


**Fig. 5.3. ESR Spectrum of 5**

All the complexes are uniformly paramagnetic with magnetic moments corresponding to one unpaired electron at room temperature (low-spin Ru(III), $t^5_{2g}$ ). The X-band EPR spectra of powdered samples of the complexes were recorded at room temperature and the EPR spectrum of the complex **5** is shown in Fig.5.3. The nature of the spectra revealed the absence of any hyperfine splitting due to interactions with any other nuclei present in the complexes. All the complexes exhibited a single isotropic resonance with g values in the range 1.99 to 2.66. Although the complexes have some distortion in their octahedral geometries, the observation of isotropic lines in the EPR spectra may be due to the occupancy of the unpaired electron in a degenerate orbital. The nature of the spectra obtained is in good experiment with that of the previously reported ruthenium (III) octahedral complexes[15].

### 5.5.4. Mass spectral analysis

The mass spectrum of the ruthenium (III) complexes is in good agreement with the proposed molecular structure $[Ru(Cl)_2(PPh_3)(L^1)]$ and $[Ru(Cl)_2(PPh_3)(L^2)]$ and the mass spectrum of the complex **5** and **8** are shown in Figs. 5.4 a and b. The molecular ion peak $[M^+]$ at m/z=769.82 and 846.65 confirms the stoichiometry of the complexes **5** and **8** respectively.

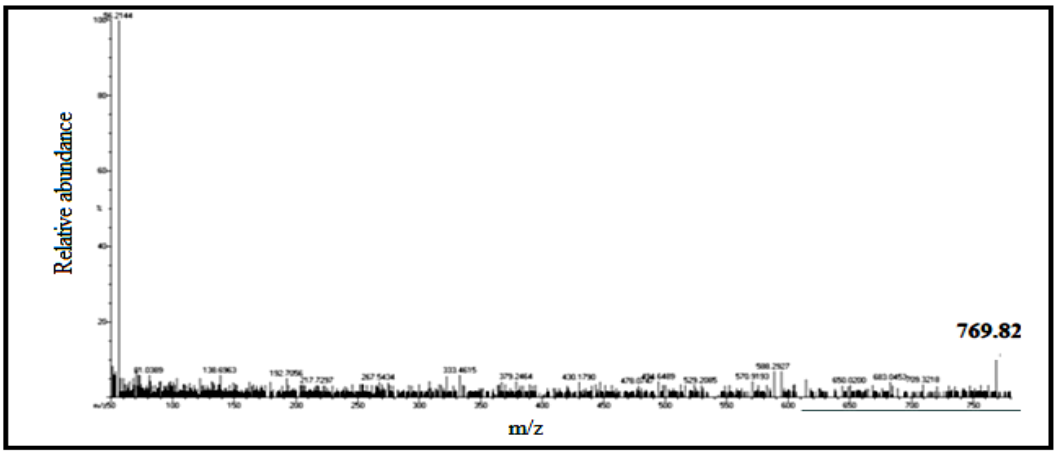


**Fig. 5.4a. EI-Mass spectrum of complex 5**

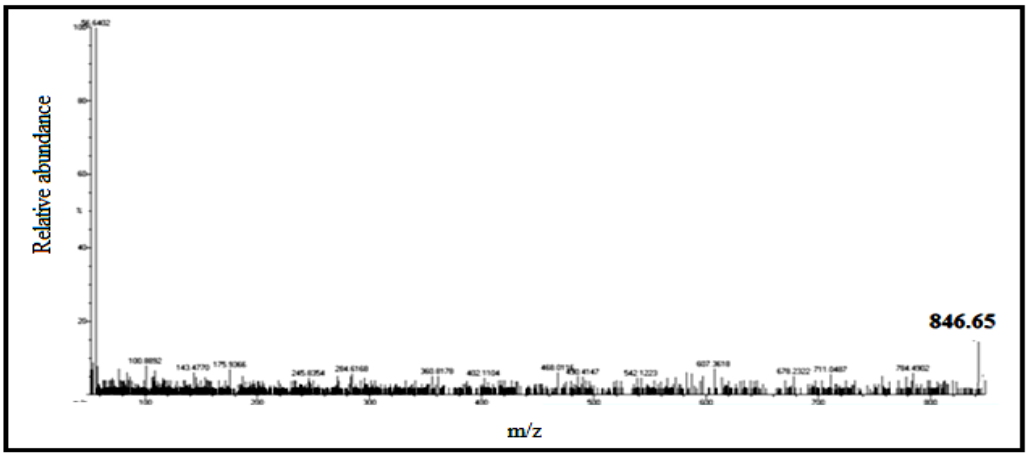


**Fig. 5.4b. EI-Mass Spectrum of complex 8**

### 5.5.5. EDX Analysis

The proposed geometry of the complexes is further confirmed from the EDX analysis. The weight percentage distribution of the elements of Ru(III) complexes is given in Table 5. 3 and the EDX spectra is given in Figs.5.5 a-d respectively.

**Table 5. 3. Weight percentage distribution of the elements of Ru(III) complexes**

| Element | 5 | 6 | 7 | 8 |
|---|---|---|---|---|

| | % Calcd | % EDX | % Calcd | % EDX | % Calcd | % EDX | % Calcd | % EDX |
|---|---|---|---|---|---|---|---|---|
| C | 49.87 | 48.63 | 44.86 | 43.12 | 46.64 | 45.98 | 53.02 | 53.17 |
| S | 4.16 | 4.10 | 4.13 | 4.01 | 4.15 | 4.10 | 4.29 | 4.06 |
| N | 9.09 | 9.18 | 7.22 | 7.35 | 9.06 | 9.34 | 7.49 | 7.56 |
| Ru | 13.11 | 12.97 | 13.02 | 13.54 | 13.08 | 12.89 | 13.52 | 13.01 |

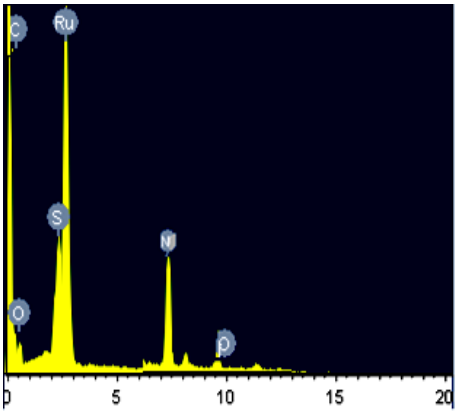


**(a)**

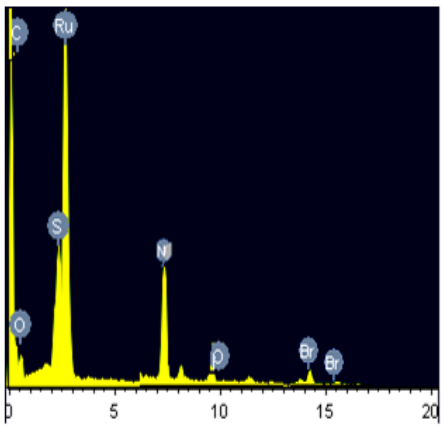


**(b)**

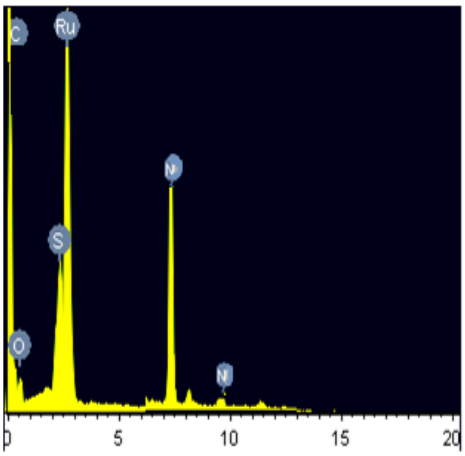


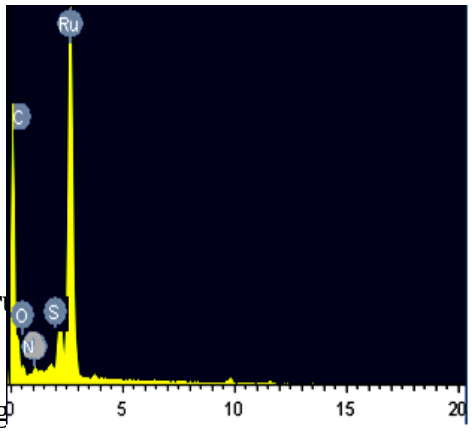


**ɔectr**

ɛating Cmin under nitrogen atmosphere and the weight loss was measured from the ambient temperature up to 800°C. The TGA data are presented in Table 5.4. From the thermogram of the complexes (Figs. 5.6a-d) it is evident that all the complexes undergo decomposition at around 130-290°C. The Schiff base ligand, $PPh_3$ and Cl are lost. Above 290°C metallic oxides alone exist. Based on the different characterization techniques and analysis, the probable octahedral structures have been proposed for all the Ru(III) complexes(Fig. 5.7).

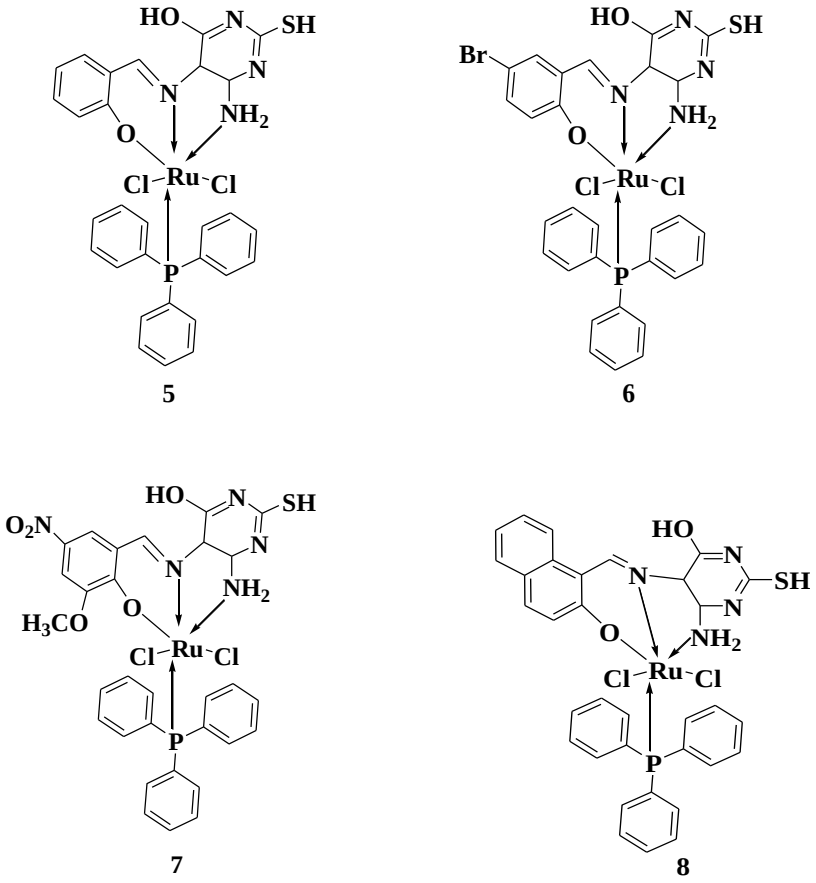


**Fig. 5. 7. Proposed geometry of the complexes**

**Table 5.4. Thermogravimetric data of the complexes**

| Complex | Decomposition Temperature ($^oC$) | Lost fragment | Residue | Weight loss % | |
|---|---|---|---|---|---|
| | | | | Calcd | Found |
| $[Ru(L_1)(Cl)_2(PPh_3)]$ | 284.35 | Schiff base, Cl, $PPh_3$ | $RuO_2$ | 86.43 | 86.02 |
| $[Ru(L_2)(Cl)_2(PPh_3)]$ | 275.95 | Schiff base, Cl, $PPh_3$ | $RuO_2$ | 84.56 | 84.31 |
| $[Ru(L_3)(Cl)_2(PPh_3)]$ | 241.89 | Schiff base, Cl, $PPh_3$ | $RuO_2$ | 85.23 | 85.89 |
| $[Ru(L_4)(Cl)_2(PPh_3)]$ | 281.34 | Schiff base, Cl, $PPh_3$ | $RuO_2$ | 83.65 | 84.10 |

### 5.5.7. DFT Calculations

#### 5.5.7.1. Geometry optimization

The DFT study has been carried out to understand the electronic structure and the magnetic interactions in the complexes. The unrestricted single point energy

calculations were done using the density functional theory method at the B3LYP level using Gaussian 09 program. The calculated bond lengths and bond angles obtained from the above calculations for Ru(III) complex are given in Table 5.5

**Table 5.5. Calculated bond angles (°) and bond lengths (Å)**

| Bond | Bond angles(°) | Bond | Bond lengths(Å) |
|---|---|---|---|
| Ru(1)-C l(2)-N(4) | 106.92 | Ru-Cl(1) | 2.422 |
| Cl(1)-Ru(1)-N(3) | 171.76 | Ru-P(1) | 2.324 |
| O(2)-Ru(1)-N(3) | 87.17 | Ru-N(3) | 2.123 |
| Cl(2)-Ru(1)-Cl(1) | 94.65 | C(5)-N(3) | 1.312 |
| O(2)-Ru(1)-P(1) | 86.92 | C(5)-H(3) | 1.090 |
| O(2)-Ru(1)-Cl(1) | 95.31 | C(2)-S(1) | 1.712 |
| O(2)-Ru(1)-N(4) | 132.61 | C(3)-O(1) | 1.252 |

The bond length of C-S in the literature is 1.749 Å for thiosemicarbazone metal complexes. In our present study the C–S bond length is 1.712 Å which is found to be in good agreement with the earlier reported value. The bond lengths of C1–C4, C5–N3, and C3–O1 bonds are equal to 1.3970, 1.312and 1.252 Å, respectively, and the double bond character of C5–N3 bond is a good evidence for Schiff base formation. The C3–O7 bond length (1.255 Å) denotes some double bond character of this bond. The calculations reveal the formation of strong hydrogen bond, H4-O1, as assumed before with bond length equal to 2.2969Å, and confirmed by the presence of the negative charge on O1 equal to 0.301e. The double band character of the bond C(3)-N(2) is reflected in the bond lengths 1.3509 Å for Ru(III) complex and 1.4005 Å for the ligand. This decrease in the bond length C(3)-N(2) in the complex shows the double bond character and therefore the tautomerism[16]. The two chlorine atoms attached to Ru(III) metal ion are cis to each other and they are shown from the bond angles. The optimized geometry of the Ru(III) complex **5** is given in Fig. 5.8.

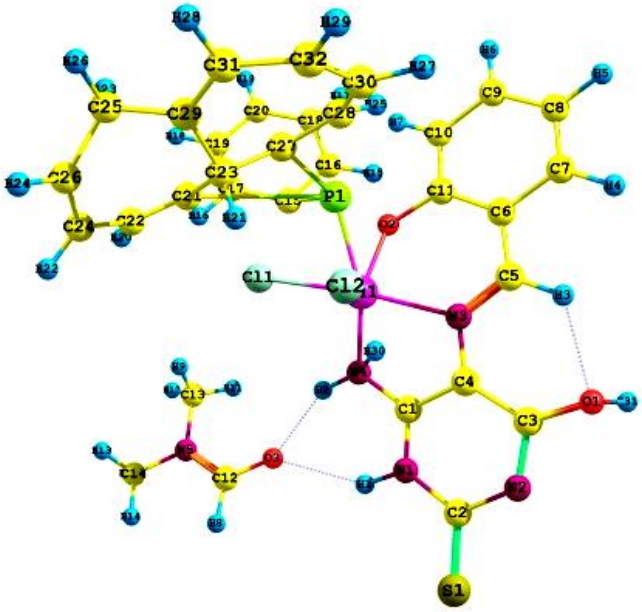


**Fig.5.8. Optimized geometry of Ru(III) complex 5**

### 5.5.7.2. Molecular electrostatic potential

Molecular electrostatic potential (MEP) is used for identifying chemical reactivities as well as presence of intra and intermolecular interactions on the skeleton of compound. Molecular electrostatic potential of ligand and complex is shown in Fig. 5.9. In these figures, different colors are used to distinguish different values of electronic potential. The red colors are correlated with electron rich area while the blue is used for representation of electron positive sites. According to Fig. 5.9 oxygen and nitrogen atoms are rich in electrons and suitable for nucleophilic attacks while in the complex, this tendency of oxygen donor atoms has been decreased[17].

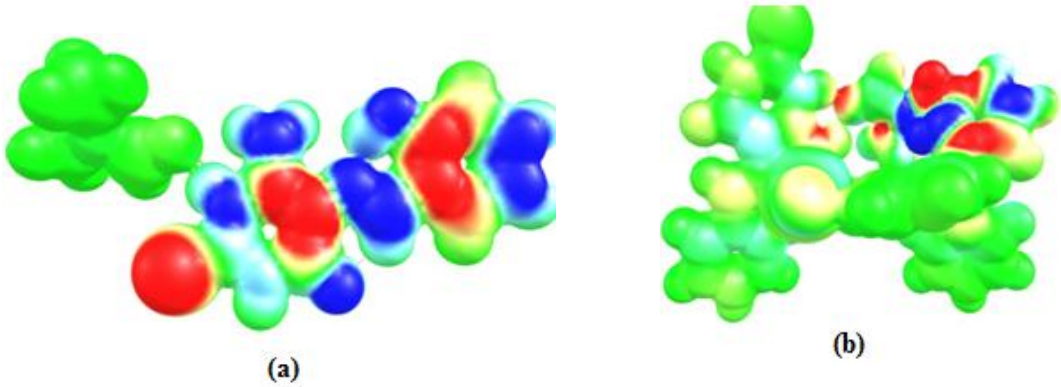


**Fig. 5.9.Molecular electrostatic potential of (a) ligand and (b) Ru(III) complex**

### 5.5.7.3. HOMO-LUMO energy gap and related molecular properties

Frontier molecular orbitals, *i.e.* the highest occupied molecular orbital (HOMO) and lowest unoccupied molecular orbital (LUMO) play an important role in the electrical properties as well as, determination of chemical reactivity. As can be seen, the electron population of HOMO and LUMO are localized on the whole skeleton of ligand **1** while in the Ru(III) complex, the electron density of HOMO is mainly located on the deprotonated Schiff base ligand and LUMO electron density is localized on the aromatic rings of heterocyclic moiety and the triphenyl phosphine. It is known that the value of $E_{HOMO}$ is often associated with the electron donating ability of the molecule, higher values of $E_{HOMO}$ is an indication of the greater ease of donating electrons to the unoccupied d orbital of the receptor. The value of $E_{LUMO}$ is related to the ability of the molecule to accept electrons, lower values of $E_{LUMO}$ shows that the receptor would accept electrons. Consequently, the value of Egap provides a measure for the stability of the formed complex on the metal surface. In the frame work of SCF MO theory, the ionization energy and electron affinity can be expressed through HOMO and LUMO energies as $I= -E_{HOMO}$, $A= -E_{LUMO}$. The hardness of the compounds depends on the gap between the HOMO and LUMO orbital energies. If the energy gap is high then the hardness is large. The global hardness $\eta= ½ ( E_{HOMO}- E_{LUMO})$. The hardness is associated with the stability of chemical potential ($\mu$) which can be expressed in combination of electron affinity and ionization potential. These calculated values are given in Table 5.6. The values of HOMO-LUMO gap is shown in Fig. 5.10.

**Table 5.6. The calculated frontier orbital energies, electronegativity, hardness and softness of ligand using UB3LYP/6-31G (d) level**

| **Compound** | $E_{HOMO}$(eV) | $E_{LUMO}$(eV) | I (eV) | A (eV) | $\chi$ (eV) | $\eta$ (eV) |
|---|---|---|---|---|---|---|
| **1** | -5.292 | -1.426 | 5.292 | 1.426 | 3.359 | 1.933 |
| **5** | -3.945 | -3.532 | 3.945 | 3.532 | 0.206 | 0.413 |

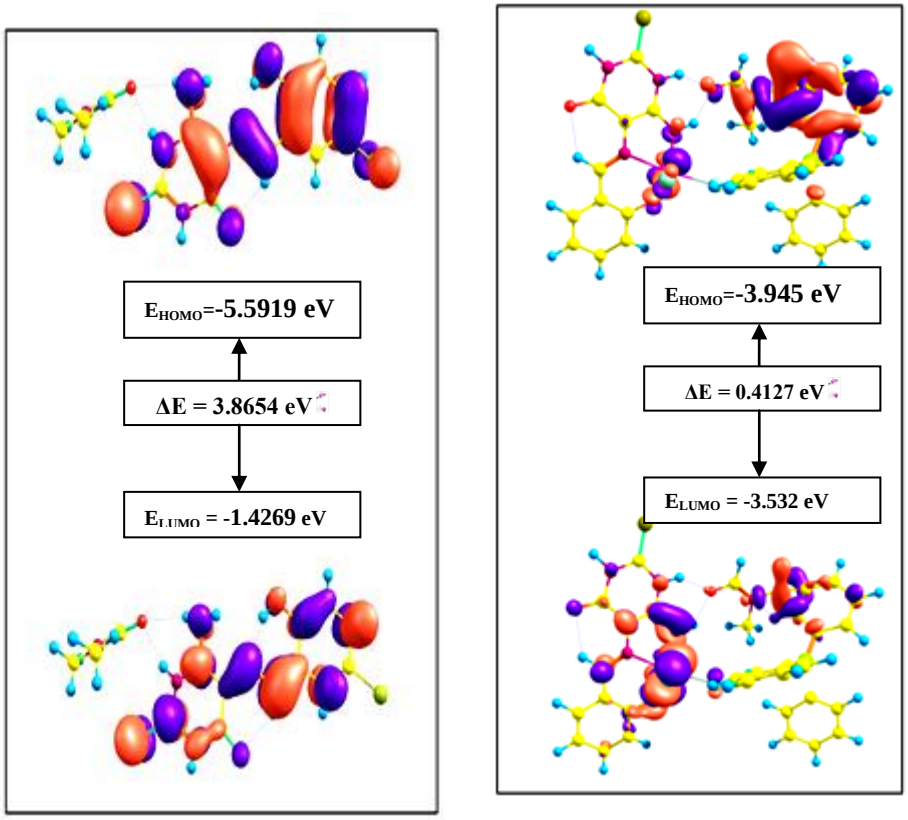


**(a)** **(b)**

**Fig. 5. 10. HOMO-LUMO gap of ligand 1 (a) and Ru(III) complex 5 (b)**

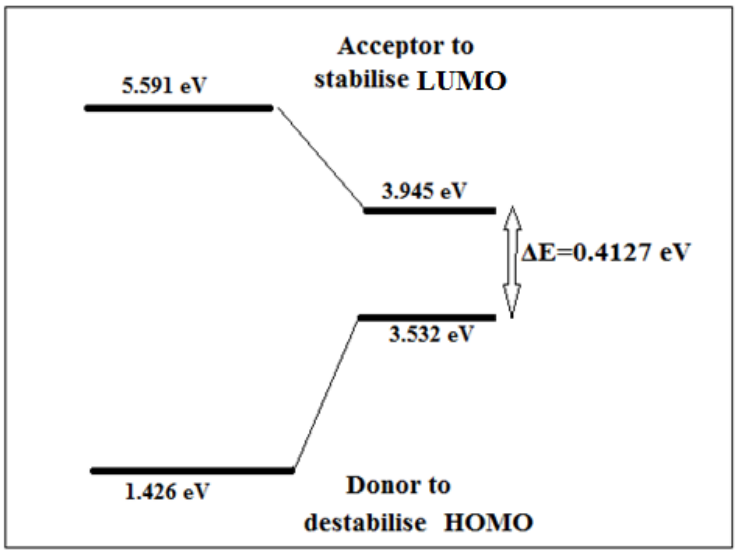


**Fig. 5.11. Energy level diagram for 5 describing HOMO-LUMO gap**

The HOMO-LUMO gap of the ligand is 3.8654eV and Ru(III) complex is 0.4127eV. The low HOMO-LUMO gap in the complex is responsible for the optoelectronic properties (light emitting diodes, thin film transistors, photovoltaic cells *etc.*,) and the physical properties of these compounds make them valuable building blocks for the development of material for OLEDs[18]. The energy level diagram explaining the HOMO-LUMO gap is shown in Fig. 5.11.

**5.6. Pharmacology**

**5.6.1. In-vitro antimicrobial activity**

The *in-vitro* antimicrobial activity of the ligand and the Ru(III) complexes were screened to evaluate their activity against *Escherichia coli, Staphylococcus aureus, Pseudomonas aeruginosa, Aspergillus niger* and *Candida albicans* and assessed them by the presence of inhibition zone (IZ) and MIC values(Table 5.7). The results showed that compared to the ligand, the complexes exhibited excellent antibacterial and antifungal activity. They were compared with standard references streptomycin/co-trimazole against the same microbes under identical experimental conditions. The results of our study showed that the complex has pronounced activity on *E.coli* and *C. albicans* and their MIC values are reported[19]. The more activity of the complex against bacteria and fungus is due to the positive charge of central metal atom shared with donor atoms of the ligand and p-electron delocalization over the whole chelate moiety hence the lipophilic nature of complex is increased. This facilitates the complex in penetrating through the lipid layers of microbial membranes, which makes a better anti-microbial agent.

**5.6.2. *In-vitro* anticancer activity**

The cytotoxicity of the Ru(III) complexes has been studied against human breast (MCF-7) cancer cells. Compounds were dissolved in DMSO and blank samples containing same volume of DMSO were taken as controls to identify the activity of the solvent in this cytotoxicity experiment. The results were analysed by means of cell viability curves and expressed with $IC_{50}$ values in the studied concentration range from 0.6 to 100μM. The activity that corresponds to the inhibition of cancer cell growth at a maximum level is shown in Figs.5.12a and b. All the complexes showed good cytotoxic activity with low $IC_{50}$ values in micromolar concentrations. The highest activity was noted for the complex **8** whereas the complex **5** showed the least activity. The ligands did not show any significant activity against HeLa thus

confirming that chelation of the ligands with the Ru(III) metal ion is responsible for the observed cytotoxic property of the complexes.

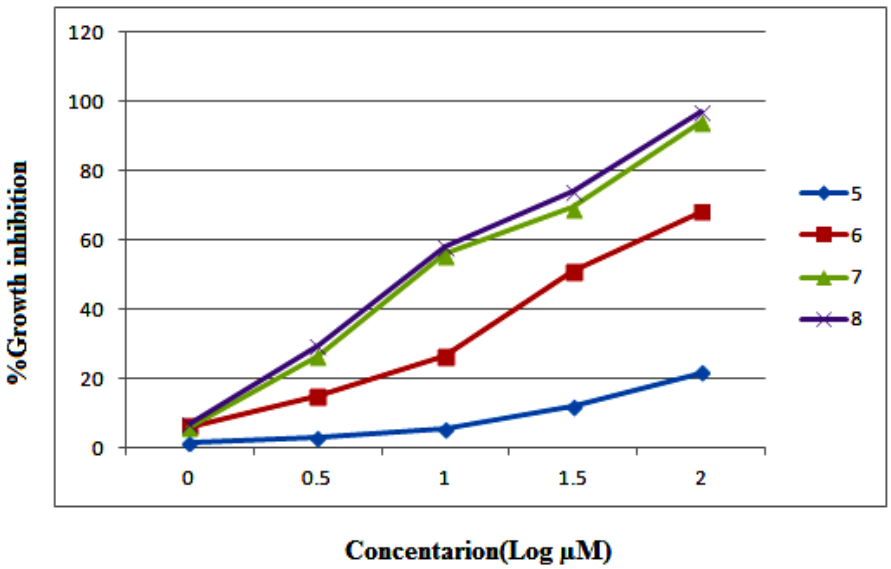


**Fig. 5.12a. Growth inhibition of HeLa cell line as a function of concentration of the compounds**

The $IC_{50}$ values of the complexes **5-8** are 79.77, 55.93, 25.85 and 21.68µg/ml respectively. Ruthenium complex tend to adopt octahedral coordination geometries versus the square planar geometries exhibited by platinum (II). Organo ruthenium complexes are appealing in drug design because, like platinum complexes, they exhibit slow rates of ligand dissociation in biological systems, allowing for a more controlled release of active drug. In drug design, ligand stability is important: fast ligand dissociation causes deactivation of the drug before it reaches target cells, resulting in a decrease in drug activity and increase in the potential for side effects.

Kinetic liability/inertness toward ligand substitution is a major determinant that controls the covalent interactions of a metal complex with biological target molecules. Ru(III) complexes probably act as pro drugs that are relatively inert toward ligand substitution and therefore their anticancer activity depends on the ease of reduction to more labile plus kinetically more reactive Ru(II) complex. The resulting Ru(II) species generally less inert, have a high propensity for ligand exchange reactions and may therefore interact with target molecules more rapidly[20].

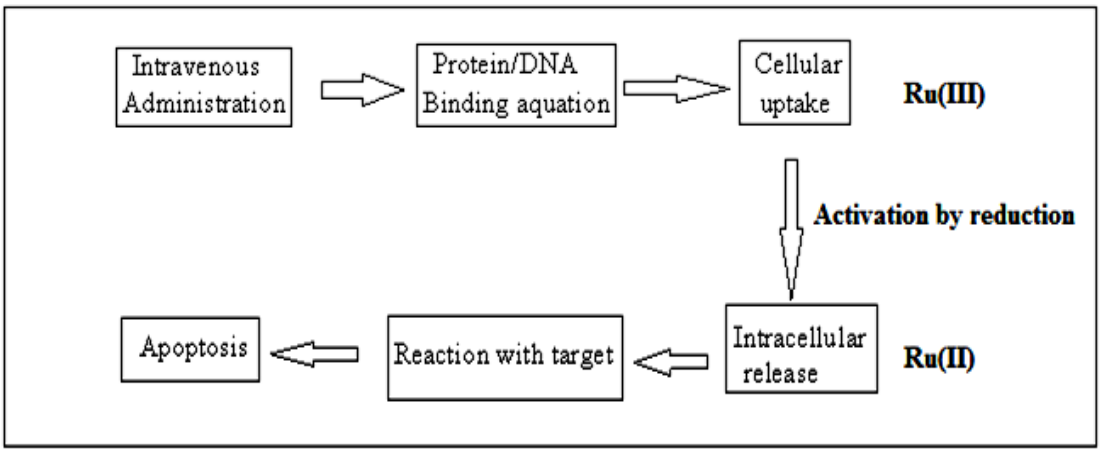


**Scheme 3: Proposed mode of action of ruthenium anticancer agents.**

### 5.6.3. Anti-tuberculosis activity

Mycobacterium tuberculosis which belongs to gram positive fast bacteria are generally slightly sensitive to environmental factors and chemicals. Such resistance results from the character of the outer cell wall containing waxy and phospholipid components bound to proteins and polysaccharides.

The synthesized Ru(III) complex were checked for its anti-tuberculosis activity and the results are reported in table 5.8 and Fig. 4.23.

**Table 5.8.** Anti-tubercular activity of the Ru(III) complex **6**

| **Compound** | **100 µg/ml** | **50 µg/ml** | **25 µg/ml** | **12.5 µg/ml** | **6.25 µg/ml** | **3.12 µg/ml** | **1.6 µg/ml** | **0.8 µg/ml** |
|---|---|---|---|---|---|---|---|---|
| **6** | S | S | S | R | R | R | R | R |

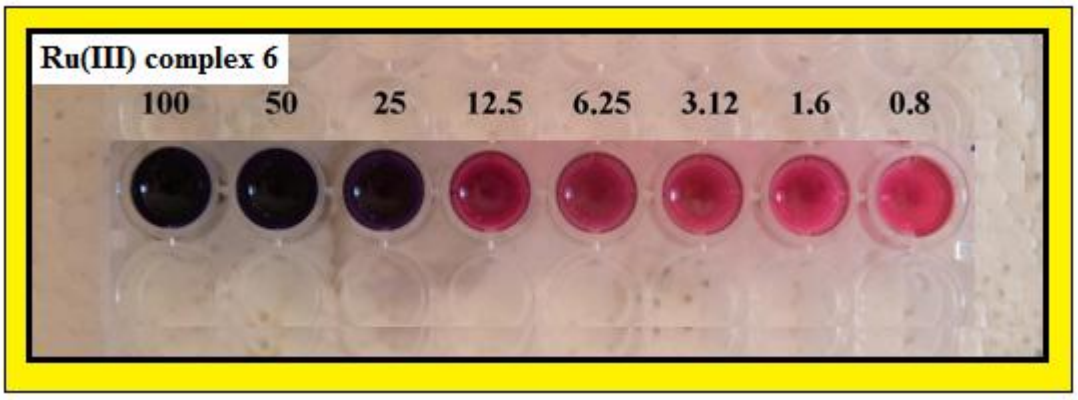


**Fig. 5.13. Anti-tuberculosis activity of Ru(III) complex 6**

The strain used for this study was *M. tuberculosis* (H37 RV strain) and the standards (MIC values) used were Pyrazinamide (3.125µg/ml), Streptomycin (6.25 µg/ml), Ciprofloxacin (3.125 µg/ml). The anti-tuberculosis activity of the Ru(III) complex is lesser than that of the standards with MIC value 25 µg/ml(Fig. 5.13).

**5.6.4. Anti-oxidant activity**

Free radicals play an important role in the inflammatory process. Many complexes have been reported as free radical inhibitors or radical scavengers in the literature. The free radical scavenging activity of the compounds, with the hope of developing potential anti-oxidants was carried out for the complexes. 2, 2'-diphenyl-2-picryl-hydrazyl (DPPH) assay is widely used for assessing the ability of radical scavenging activity and it is measured in terms of $IC_{50}$ values. Due to the presence of odd electron, DPPH shows a strong absorption band at 517nm in the visible region. As this electron becomes paired off in the presence of free radical scavenger, this absorption vanishes and the resulting decolourisation is stoichiometric with respect to the number of electrons taken up. The DPPH assay of the complexes shown in Fig. 5.14 shows that the complexes exhibited moderate activity than the standard ascorbic acid (Aca). The $IC_{50}$ values indicated that the compounds showed antioxidant activity in the order **7>6>8>5.** Complex **7** exhibited higher anti-oxidant activity than the other complexes.

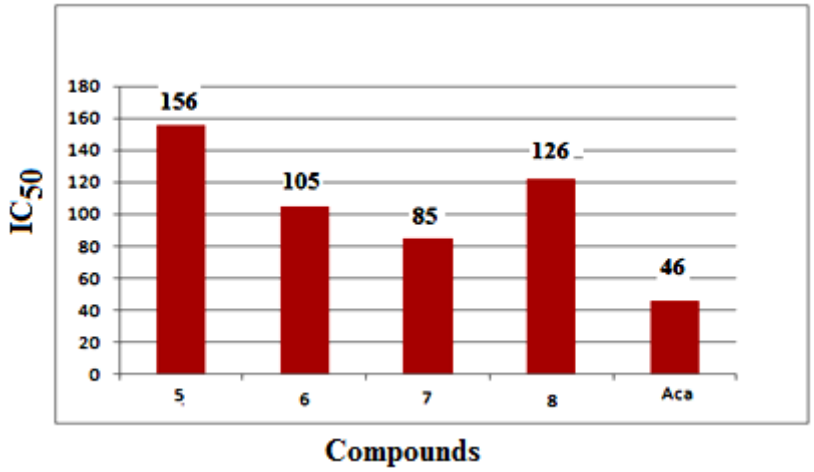


**Fig. 5. 14. Antioxidant activity of the compounds 5-8 with standard ascorbic acid.**

**5.6.5. DNA Binding**

### 5.6.5.1. Absorption spectral measurements

Interaction of metal complex compounds with DNA is taken as an important initial signal for evaluation of biological properties of a compound. Activity of ruthenium compounds towards DNA, as a key target for anticancer drugs, may originate from either their covalent interaction with DNA nucleobases or non-covalent binding such as electrostatic interaction of positively charged species with phosphate backbone and intercalation as well. Electronic absorption is a very useful method to determine the binding properties of metal complexes with DNA. Spectroscopic study of interaction of the complexes with CT DNA was performed by titration of fixed concentration of complex compounds with increasing concentrations of calf thymus DNA (CT DNA) in the [DNA] / [complex] ratio range 0−2.88 and 0−3.51, respectively. The binding constants, *K*b were calculated on the basis of the equation mentioned in chapter 4 . Weak bathochromic shifts, hypochromism and constant binding values of order $10^4$ $M^{-1}$ indicate that both compounds, containing Schiff bases derived from various aldehydes act as moderate DNA-intercalators. Generally, hypochromism and hyperchromism are the two spectral features which are closely connected with the double helix structure of DNA. The observation of hypochromism is indicative of intercalative mode of binding of DNA to the complexes along with the stabilization of the DNA double helix structure. The magnitude of the hypochromism and red shift depends on the strength of the interaction between the DNA and the complex. The binding constants of the complexes **5** to **8** range from $1.7X10^4$ $M^{-1}$, $4.8$ $X10^4$ $M^{-1}$, $5.7$ $X10^5$ $M^{-1}$, $4.3$ $X10^5$ $M^{-1}$ respectively. The observed values of $K_b$ reveals that the ruthenium (III) complexes bind strongly than the respective ligands to DNA *via* intercalation[21,22]. The order of binding affinity is **7>8>6>5.** The absorption spectra showing the changes in the order of increasing concentration is shown in Figs. 5.15a-d respectively.

### 5.6.5.2. Fluorescence spectral measurements

The fluorescence titration experiment has been widely used to characterize the compound-DNA interactions, in which the fluorescence emissions of interacting compounds can be quenched, which results in the decrease of fluorescence intensity. On the other hand, in some compounds, the compound-DNA interactions can prevent the compound fluorescence emission from being quenched by polar solvent molecules. Consequently, the fluorescence intensity increases. In this study, the interactions between the compounds and CT-DNA were investigated by fluorescence

titration. The results are shown in Fig 5.16a-d. Specifically, the fluorescence intensity of compounds **5-8** decreased when titrated by CT-DNA, being in good agreement with the fluorescence behavior of other intercalators reported in the literature.

**EB Competition Assay**

The well-established quenching assay based on the displacement of the intercalating dye, ethidium bromide (EB), from CT-DNA was employed to further investigate the interaction mode between the complexes and CT-DNA. EB is a very useful DNA structural probe, which shows a significant increase in fluorescence intensity when intercalating into the base pair of DNA. However, the enhanced fluorescence can be quenched evidently when there is a second complex that can replace the bound EB or break the secondary structure of DNA. It has been reported that the groove DNA binders can also cause the decrease in EB emission intensities. The effects were, however, only moderate. Before we started the fluorescence test of the compounds with DNA, we tried different excitation wavelengths from 280 to 550 nm and found only one fluoresce for each compound, and each had a fixed wavelength, so we chose the excitation wavelength that is similar with the UV absorbance one. The EB competition assay results and the plot for the calculation of binding constant are shown in Fig. 5.16e-h. The fluorescence intensity of DNA-bound EB at 526 nm decreased remarkably with an increase in the concentration of the compounds (**5-8**). This decrease in fluorescence intensity may be due to the quenching of some EB molecules that were released from DNA into the solution after being replaced by the compounds. The similar phenomenon that the fluorescence of DNA-bound EB was quenched as a result of the DNA and compound interactions is a characteristic sign of intercalation. The fluorescence quenching of DNA-bound EB can be well described by the linear Stern-Volmer equation in which the synthesized compounds were the quenchers[23]:

$$I_0/I = 1 + K_{SV}[Q]$$

$I_0$ and I represent the fluorescence intensities in the absence and presence of quencher, respectively; $K_{SV}$ is a linear Stern-Volmer quenching constant; Q is the concentration of quencher. The $K_{SV}$ values were given by the ratio of the slope to intercept. The $K_{SV}$ values for the tested compounds are $2.3X10^4$ $M^{-1}$, $3.7\ X10^4$ $M^{-1}$, $4.8\ X10^5$ $M^{-1}$, $5.2\ X10^5$ $M^{-1}$.

**5.6.6. Docking with DNA**

To obtain further support for the above DNA binding modes suggested on the basis of experimental results, the binding energies for the interaction of the Ru(III) complex **5** with the sequence the duplex DNA D(*CP*GP*CP*GP*AP*AP*TP*TP*CP*GP*CP*G)-3') dodecamer was taken from the Protein Data Bank (PDB ID: 1BNA) and used in docking studies. All possible docking poses were considered and the docking was performed and the complex-DNA interactions and the non-covalent interactions are given in Fig. 5.17. Among several modes of interactions, intercalation seems to be the most favorable mode of DNA binding for the interaction of Ru(III) complex with DNA. The binding energy of the the complex is -8.56 Kcal/mol with a $pIC_{50}$ value of 533.55 nanomolar concentration. Thus the Ru(III) complex **5** with DNA intercalates in the minor groove which is in accordance with the experimental results from absorption spectral measurements.

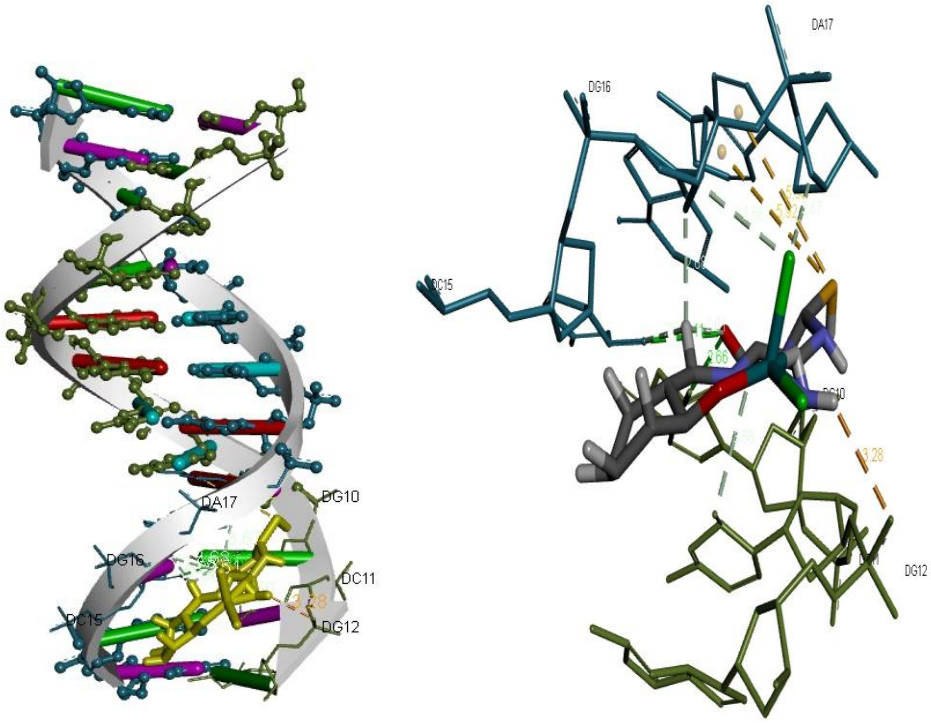


**Fig. 5.17: Docking poses of the Ru(III) complex 5 with DNA**

### 5.6.7. Nuclease activity in the presence of radical scavengers

Artificial nucleases typically produce a sequential transition between super-coiled (I), single-nicked (II) and double-nicked (III) DNA. Each scission changes the overall structure of the DNA fragment and is thus identifiable *via* gel electrophoresis. Super coiled DNA (I) is the native, uncut plasmid DNA that is

obtained from *Escherichia coli*, appears as the band of lowest mass and travels the furthest on the gel; single-nicked (II) represents a form of relaxed DNA in which only one strand is cleaved, its relaxed form causes it to appear as the band of highest mass and travel the shortest distance on the gel; and double nicked (III), represents a linearized plasmid with both strands cleaved and appears between the super coiled and single nicked bands.

There are two possible mechanisms known to play a role in the cleavage by metallonucleases: hydrolytic and oxidative. The hydrolytic mechanism of cleavage relies on the inductive effects of the metal on the phosphate backbone. This interaction increases the susceptibility of the phosphate backbone toward nucleophilic attack by bulk water or hydroxide thus producing the linearization of DNA observed as a result of complex cleavage. The oxidative mechanism of cleavage functions primarily through the production of reactive oxygen species (ROS) and can include hydroxyl radical (•OH) due to the reaction between the metal complex and oxidant which can be explained as shown below. The cleavage efficiency was measured by determining the ability of the complex to convert the supercoiled DNA (Form I) to open circular form or nicked form(Form II). The metal complexes after binding to DNA can induce several changes in the DNA conformation, such as bending, local denaturation, intercalation, micro loop formation and subsequent DNA shortening lead to decrease in molecular weight of DNA. The ability of metal complexes to perform DNA cleavage is generally monitored by agarose gel electrophoresis and in the present work pBr322-DNA was chosen to investigate its cleavage.

$$M(III)\,L + e^- \rightarrow M(II)\,L$$

$$M(II)\,L + O_2 \rightarrow M(II)\,L + O_2^-$$

$$2O_2^- + 2H^+ \rightarrow H_2O_2 + O_2$$

$$M(II)\,L + H_2O_2 \rightarrow M(II)\,L + OH^- + OH\cdot$$

$$O^{2-} + H_2O_2 \rightarrow O_2 + OH^- + OH\cdot$$

The cleavage experiments were carried out in the absence and presence of activating agent, $H_2O_2$ under aerobic conditions and are shown in Fig. 5.18 showing the hydrolytic cleavage of the complexes **6-10** at 40μM. A control experiment using DNA alone does not show significant cleavage of DNA (Lane 1). Further, when DNA is allowed to interact with the complexes, no considerable difference in the intensity of

the bands for metal bound DNA as compared to control DNA was observed. This result suggests that the nuclease activity of the complexes does not involve hydrolytic pathway. These experimental facts demonstrated that a combination of both the ruthenium complexes and the activating agent, $H_2O_2$ are required to show any significant cleavage. Complex **5** and **7** show both forms, **6** and **8** show significant cleavage than the ligands. The synthesized ligand **1** in lane 6 do not show any cleavage activity[24, 25].

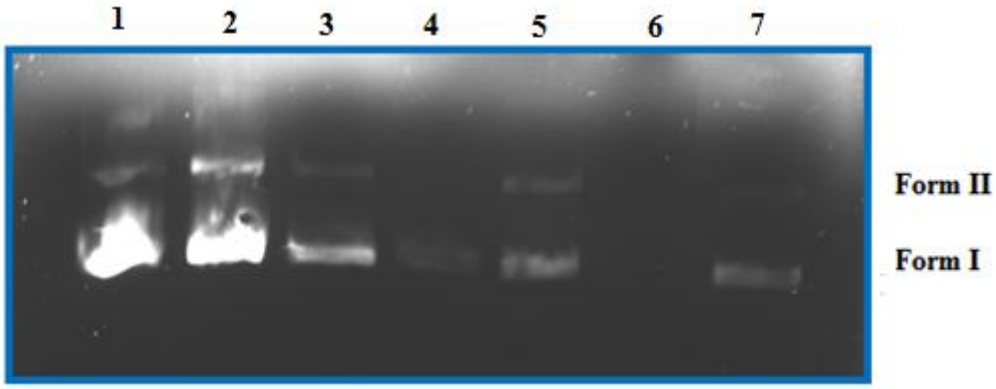


**Fig. 5.18. Changes in the agarose gel electrophoretic pattern of pBr322 DNA induced by $H_2O_2$ and Ru(III) complexes , lane 1, DNA alone; lane 2, DNA + $H_2O_2$; lane 3, DNA + 5 + $H_2O_2$; lane 4, DNA + 6 +$H_2O_2$; lane 5, DNA + 7+ $H_2O_2$; lane 6, DNA + 1 + $H_2O_2$; lane 7, DNA+8+$H_2O_2$.**

### 5.7. Catalytic activity

The catalytic activity of the newly synthesized ruthenium(III) complexes was examined in the presence of hydrogen peroxide as the co-oxidant for the oxidation of primary and the secondary alcohols in $CH_2Cl_2$ at ambient temperature[26]. Benzaldehyde, cyclohexanone, cinnamaldehyde and butyraldehyde were formed from the corresponding alcohols after refluxing for about 2h, and then quantified as 2,4-dinitrophenyl hydrazone derivatives. The relatively higher yield obtained for oxidation of cinnamyl alcohol compared with benzyl alcohol, cyclohexanol and n-butanol was due to the fact that the α-CH unit of cinnamyl alcohol is more acidic than the other alcohols used for our reaction and there is retention of C=C double bond. The order of the catalytic activity of the alcohols in the presence of Ru(III) complex synthesized is cinnamyl alcohol>benzyl alcohol>cyclohexanol>n-butanol. The order of reactivity of the synthesized complexes is $[Ru(L_2)(Cl)_2(PPh_3)]$>

$[Ru(L_3)(Cl)_2(PPh_3)]$>$[Ru(L_1)(Cl)_2(PPh_3)]$≈ $[Ru(L_4)(Cl)_2(PPh_3)]$. The oxidation of alcohols by ruthenium(III) complexes is given in Table 5.9.

**5. 8. Conclusion**

In this chapter, we have described the synthesis of Ru(III) complexes with pyrimidine based Schiff base ligand with $PPh_3$ as the co-ligand. The structures of these complexes were confirmed by spectral and elemental analysis. The optimized geometry of the complexes has been studied using Gaussian 09 program. The HOMO-LUMO energy values and their value has been calculated and found to be lesser for the complexes than the ligand. The pharmacological activity of the ligand and the complexes has been screened and found to be good and their results has been discussed. The DNA binding studies has been done using absorption and emission spectral measurements. The The binding constants calculated show that the complexes are moderate intercalators. The ability of metal complexes to perform DNA cleavage is generally monitored by agarose gel electrophoresis and in the present work pBr322-DNA was chosen to investigate its cleavage and the mechanism is found to be oxidative. The catalytic activity of the complexes has been studied and their order of reactivity The order of reactivity of the synthesized complexes is $Ru(L_2)(Cl)_2(PPh_3)]$> $[Ru(L_3)(Cl)_2(PPh_3)]$>$[Ru(L_1)(Cl)_2(PPh_3)]$≈ $[Ru(L_4)(Cl)_2(PPh_3)]$.

**References**


1. Durig J R, Danneman J, Behnke W D, Mercer E E, *Chem.-Biol. Interact*, **13** (1976) 287.
2. Clarke M J, *Met Ions Biol Syst* **11** (1980) 231.
3. Clarke M J, Zhu F, Frasca D R, *Chem Rev*, **99** (1999) 2511.
4. Keppler B K, Wehe D, Endres H, Rupp W, *Inorg Chem*, **26** (1987) 844.
5. Keppler B K, Rupp W, Juhl U M, Endres H, Niebl R, Balzer W, *Inorg Chem,* **26** (1987) 4366.
6. Keppler B K, Rupp W, *J Cancer Res Clin Oncol* **111** (1986) 166.
7. Garzon F T, Berger M R, Keppler B K, Schmaehl D, *Cancer Chemother. Pharmacol.* **19** (1987) 347.
8. Mestroni G, Alessio E, Sava G, Pacor S, Coluccia M, Boccarelli A, *Met-Based Drugs* **1** (1994) 41.
9. Mohammed subarkhan M, Ramesh R, *Spectrochim Acta & Mol Biomol Spectroscop*, **138** (2015) 264.

10. Ramesh R, Dharmaraj N, Karvembu R, Natarajan K, *Indian J Chem*, **39A** (2000) 1079.
11. Vishwanathamurthi P, Geetha A, Karvembu R, Natarajan K, *Indian J Chem*, **44A** (2005) 90.
12. Prasanna N, Srinivasan S, Rajagopal G, Athappan P R, *Indian J Chem*, **40A** (2001) 426.
13. Sharma V K, Srivatsava A, Srivatsava S, *J Serb Chem Soc*, **71** (2006) 917.
14. Manimaran A, Jayabalakrishnan, *J Adv Res*, **3** (2012) 233.
15. Priyarega S, Prabahkaran R, Aranganayagam, Karvembu R, Natarajan K, *Appl Organometal Chem*, **21** (2007) 788.
16. Akbari A, Jalili Rasti M, *Computational Res*, **1** (2013) 27.
17. Yousef S, Shekhshoaie I, Fromm K M, *J Mol Struct*, **1072** (2014) 267.
18. Al-Moren M, Alaghaz A M A, *Int J Electrochem Sci*, **8** (2013) 8669.
19. Amer S, El-Wakiel N, El-Ghamry H, *J Mol Struct*, **1049** (2013) 326.
20. Kamatchi T S, Chitrapriya N, Lee H, Fronczek C F, Natarajan K, *Dalton Trans*, **41** (2012) 2066.
21. Ying P, Tian X, Zeng P, Lu J, Chen H, Xiao M, Med Chem, **4** (2014) 8.
22. Sathiyaraj S, Ayyannan G, Jayabalakrishnan C, *J Serb Chem Soc*, **79** (2014) 151.
23. Zhao J, Li W, Ma R, Chen S, Jiang T, *Int J Mol Sci*, **14** (2013) 16851.
24. Dar A M, Ahmad M S, Gatoo M A, *J Biomed Res Ther*, **4** (2015) 3.
25. Raman N, Dhaveethuraja J, Sakthivel A, *J Chem Sci*, **119** (2007) 303.
26. Gunasekaran N, Remya N, Radhakrishnan S, Karvembu R, *J Co-ord Chem*, **64** (2011) 491.